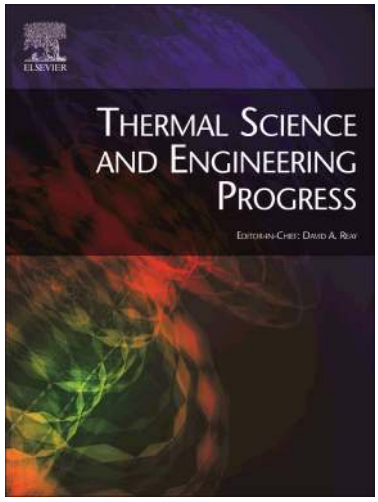

Numerical simulation of thermal and residual stress fields induced by lined pipe welding

Obeid Obeid, Giulio Alfano, Hamid Bahai, Hussam Jouhara

PII: S2451-9049(17)30267-6
DOI: https://doi.org/10.1016/j.tsep.2017.10.005
Reference: TSEP 69

To appear in: *Thermal Science and Engineering Progress*

Received Date: 27 August 2017
Revised Date: 2 October 2017
Accepted Date: 5 October 2017

Please cite this article as: O. Obeid, G. Alfano, H. Bahai, H. Jouhara, Numerical simulation of thermal and residual stress fields induced by lined pipe welding, *Thermal Science and Engineering Progress* (2017), doi: https://doi.org/10.1016/j.tsep.2017.10.005

Numerical simulation of thermal and residual stress fields induced by lined pipe welding

Obeid Obeid[1, a], Giulio Alfano[1,b], Hamid Bahai[1,c], Hussam Jouhara[1,d]

[1]College of Engineering, Design and Physical Sciences, Brunel University, UB8 3PH Uxbridge, UK

[a]obeid.obeid@brunel.ac.uk, [b]giulio.alfano@brunel.ac.uk, [c]hamid.bahai@brunel.ac.uk, [d]hussam.jouhara@brunel.ac.uk

ABSTRACT

This paper investigates numerical thermal fields and residual stresses induced by single-pass weld overlay (lap-weld) and girth welding (butt-weld) in lined pipe using Tungsten Inert Gas (TIG) welding. A distributed power density of the moving heat source based on Goldak's ellipsoid heat flux distribution is used in a Finite Element (FE) simulation of the lined pipe welding process. In addition, radiation and convection have been incorporated in heat transfer coefficient user-subroutines for the FE code ABAQUS. The 3-D FE model approach has been validated using previous experimental results published for butt-welds of similar sections of carbon-manganese C-Mn steel pipe lined with stainless steel. The FE model has been developed to determine the thermal isotherms and residual stress distributions from weld overlay and girth welding. The use of an inner layer known as a liner has a considerable influence on the thermal history and residual stress distributions. Furthermore, the influence of the weld overlay has been examined thermally and mechanically as it is a key factor that can affect the quality of lined pipe welding.

Keywords: Lined pipe; Weld overlay; Girth welding; Thermal history; Residual stresses

Nomenclature

a	Half-length of heat source (mm)
	Depth of heat source (mm)
	Half-width of heat source (mm)
c	specific heat capacity (kJ/kg K)
$d\varepsilon^{\cdot}$	Plastic strain increment
$d\sigma$	Stress increment (Pa)
h_{con}	Convective heat transfer coefficient (W/m^{2}K)
H	Enthalpy of material (J/kg)
H	Strain-hardening rate (Pa)
	Current (Amperes)
NT11	Temperature (°C)
	Power density (Wm^{-3})

	Total heat input (W)
	Radial distance of the heat torch centre from the pipe axis (mm)
S, S33	Axial residual stress (N)
	Current time (s)
	Initial time (s)
I	Current temperature
I_{amb}	Ambien temperature (°C)
v	Welding speed (mm/s)
	Voltage (volts)
WCL	Weld centre line
ε	Total strain
ε^{-}	Elastic strain
ε_{em}	Effective radiation emissivity
ε^{-}	Plastic strain
ε^{-}	Thermal strain
	Angle of moving torch around the pipe (Rad)
κ	Conductivity (W/mK)
	Welding efficiency (%)
ρ	Density (kgm^{-3})
σ_{bol}	Stefan-Boltzmann constant
υ	Poisson's ratio
	Angular velocity (Rad/s)

1. Introduction

For hydrocarbon pipelines where the production fluid is corrosive such as H_2S (sour service) or CO_2 (sweet service), C-Mn steel pipes are usually not suitable. One alternative is lined pipe consisting of an inner layer (the liner) and outer layer (backing steel). The liner is made of corrosion resistant alloy (CRA) such as Alloy625, 304 and 316L stainless steel (SS) whilst the backing steel is made of low-cost carbon steel [1].

Lined pipe welding is a complex process requiring two sequential welds. The liner is typically fixed using weld overlay to seal its end with the outer pipe. Consequently, no gap is left between the liner and the backing steel [2]. A girth weld is then executed to join two adjacent lined pipes. The integrity assessment and lifetime estimation of the lined pipe require consideration of thermal fields and residual stresses induced by such welded structures. A computational procedure based on FEM is an effective alternative to experiments [3]. There are many obstacles which make the experimental investigation of lined pipe welding inflexible, time consuming and prohibitively expensive.

It has been over 25 years since Karlsson and Josefson [4] first proposed a full three-dimensional thermal and mechanical study of circumferential butt-welding operations. Their C-Mn single-pass model using FE-code (ADINAT/ADINA) was validated experimentally by other similar work [5, 6]. Developing the finite element code ABAQUS for non-linear

analysis enabled Brickstad and Josefson [7] to numerically simulate a series of multi-pass girth-butt-welded stainless steel joints.

Over the last decade or so, a significant development of FE codes in 3-D FE modelling has given a high flexibility in predicting the thermal history and residual stresses in a butt-welded steel pipe. Deng and Murakawa [8] developed 3-D and 2-D FE models to analyse temperature history and residual stresses in multi-pass girth welds with SUS304 stainless steel pipe sections. Their results of 3-D modelling obtained from ABAQUS are in very good agreement with experimental measurements. Akbari and Sattari [9] developed an FE dissimilar cylindrical model in which one joint is made of A240-TP304 stainless steel and the other one is A106-B carbon steel. The thermo-mechanical behaviour and the effect of heat input on the residual stress distribution were discussed in that study. The numerical results obtained by the ANSYS code showed good agreement with the experimental ones using the hole-drilling method.

The thermal and mechanical analyses depend on several principal factors such as material properties, heat input, welding pool geometry, boundary conditions and welding sequence. Subsequently, Deng et al. [10] tried to validate a welding simulation for dissimilar materials consisting of a low alloy steel pipe and an austenitic stainless steel pipe. Some discrepancy between the numerical and the experimental results were found because the weld cladding layer under the low alloy steel joint was not taken into account in the dissimilar materials welding simulation.

There are a limited number of studies in the literature which have reported lined pipe welding simulation due to the complex sequence of weld overlay and girth welding. Even so, it is worth noting that the technique used to move the heat source around the weld overlay to fix and seal the liner at the pipe ends and then around the girth weld to join two specimens of lined pipe has not been reported yet. Consequently, Obeid et al. [11] presented a new procedure to simulate a typical lined pipe process including the weld overlay and girth welding. Furthermore, a sensitivity analysis to determine the influence of the cooling time between weld overlay and girth welding and of the welding speed has been conducted thermally and mechanically. In this study, a three-dimensional FE model is developed using ABAQUS [12] to study the thermal and mechanical behaviour induced by the weld overlay and girth welding process, described here as Case A. The numerical approach presented is validated thermally and mechanically by previously published experimental results. Moreover, thermal and mechanical results in the corresponding cases without considering

weld overlay, described as Case B, and without liner, described as Case C, were also examined for comparison with Case A.

2. FE modelling

The thermal history fields and the resulting residual stresses are obtained by simulating the weld overlay and the girth welding using ABAQUS 6.13-1 and FORTRAN codes [12]. The procedure consists of two analyses, thermal and mechanical. The first analysis is executed to produce the thermal history of the whole thermal model. In the following analysis, the thermal distribution at each node of the thermal model is employed as a thermal load on the corresponding node in the mechanical analysis in order to determine the stress distribution at this node.

2.1. Finite element mesh

Due to the symmetry of the lined pipe, only one of its two components is modelled. The three-dimensional FE model contains a total of 51840 nodes associated with 10560 elements. Among these, 17400 nodes and 2400 elements represent the liner geometry and the remaining 10560 elements represent the backing pipe geometry.

A fine mesh has been considered in the fusion zone (FZ) and its vicinity, i.e. in the heat affected zone (HAZ), because of the higher gradients of temperature and flux. The element size increases with an increase in the distance from the welding centreline (WCL), in both the C-Mn pipe and the liner. There are 120 sets of divisions in the circumferential direction. Furthermore, the thickness of lined pipe consists of four layers of elements. Three of these layers are for the C-Mn pipe and a one layer is for the liner as shown in Fig. 1.

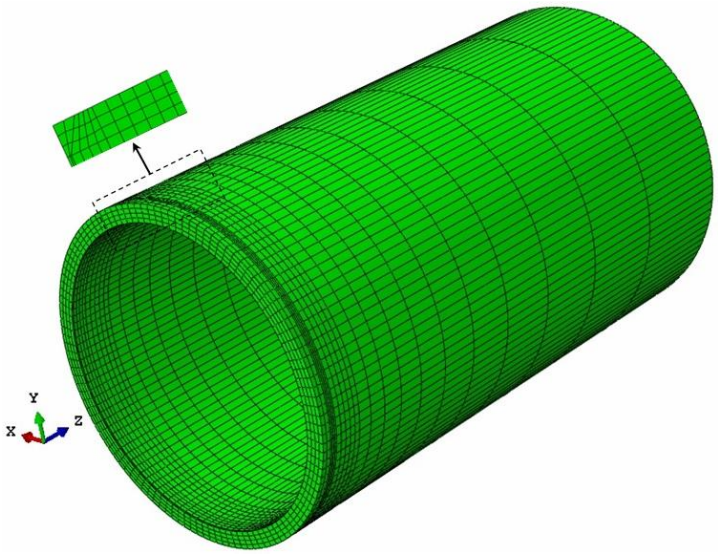

Fig.1. Three-Dimensional FEM.

The FE mesh applied in the structural analysis is the same as that used in the thermal analysis. Nevertheless, both analyses have different element types and boundary conditions. 20-node quadratic hexahedral heat-transfer elements with a single degree of freedom, named DC3D20 in ABAQUS, are used for the thermal analysis. Continuum solid, three-dimensional 20-node reduced integration elements (C3D20R) are employed for mechanical analysis with three translation degrees of freedom in combination with a large displacement (nonlinear geometry).

2.2. Thermal analysis

Transient heat-transfer analysis is executed to evaluate the thermal distributions during welding. Basically, there are two choices for boundary conditions, either specifying the flux or the temperature. In this case, the energy balance for each domain is governed by the classical energy balance equation given as [13]:

$$\rho \frac{\partial H}{\partial t} - \nabla.(\kappa \nabla T) = q(x,y,z,t) \tag{1}$$

where ρ denotes the density of the materials, H represents the enthalpy (per unit volume), t is time, T is the temperature, the material thermal conductivity which is assumed to be isotopic is denoted by $\kappa = \kappa(T)$ and $q = q(x,y,z,t)$ is the welding volume heat input. The enthalpy in Eq. (1) is given as:

$$H(T) = \int_{T_{ref}}^{T} C\, dT + l\, f_1(T) \tag{2}$$

where C and l are the specific heat capacity and latent heat, respectively, $\mathrm{T_{ref}}$ is an arbitrary reference temperature, and $\mathrm{f_1}$ is the volumetric liquid fraction known as a characteristic function of temperature, defined as:

$$f_1(T) = \begin{cases} 0 & T < T_{solid} \\ \dfrac{T - T_{solid}}{T_{liquid} - T_{solid}} & T_{solid} \le T \le T_{liquid} \\ 1 & T > T_{liquid} \end{cases} \tag{3}$$

where T_{solid} and T_{liquid} are the solidus and liquidus temperatures, respectively. It is clear that the latent heat is assumed to be in addition to the specific heat effect during phase change. The specific heat is the amount of energy required to change the temperature of 1 kg of the

material by 1°C. The specific heat is also assumed to be constant (without change in temperature) during phase change.

Accounting for the rotational movement of the welding torch along the circumference, the power density can be given as a function of position and time as follows [11]:

$$q(x,y,z,t) = \frac{6Q\sqrt{3}}{abc\pi\sqrt{\pi}} e^{-3(x-(R\sin\theta+x_0))^2/a^2} e^{-3(y-(R\cos\theta+y_0))^2/b^2} e^{-3(z-z_0)^2/c^2} \quad (4)$$

where $Q = IV\mu$ is the energy input rate which is given by the product of the current I, voltage V and the weld efficiency μ, R is the radial distance of the heat torch centre from the pipe axis, θ is the angle from the start/stop point (where θ = 0°) at which the torch has travelled around the pipe. Parameters a, b and c are the semi-axes of the ellipsoidal welding pool in directions, x, y and z, respectively. Denoted by ω, the angular velocity is used in welding which results in values represented by $\theta = \omega(t - t_0)$, where t is the current time and t_0 is the initial time of the analysis.

Eq. (4) has been implemented in ABAQUS by coding the FORTRAN DFLUX user-subroutine [12]. The position of the weld torch is calculated first in DFLUX according to the welding time t. Thereafter, the power density q is computed at each integration point.

In the present work, a moving heat torch with the element birth technique is applied, where the elements of the weld bead are deposited sequentially. This procedure initially requires the deactivation of all elements representing the welds. Then, the deactivated element sets are re-activated in successive steps as the heat source passes through those sets. The bead elements that have not been deposited yet, are given a value for thermal conductivity, equivalent to that of air [14]. The thermal conductivity returns to the conductivity of steel as the weld bead is deposited. Eventually, the weld simulation is complete and the whole pipe is allowed to cool down to either inter-pass temperature or room temperature after weld overlay or girth welding, respectively.

During the thermal analysis, both convection and radiation are taken into account as boundary conditions. In particular, radiation heat losses are dominant in the FZ and its vicinity, whereas convection heat losses are dominant away from the weld zone at lower temperatures [15]. Due to the fact that there are two different base materials (C-Mn and SUS304), two heat transfer coefficients are considered. Each heat transfer coefficient

represents a combination of convection and radiation. For carbon steel surfaces, the total heat transfer coefficient can be written as [16]:

$$h_{carbon} = h_{con} + \varepsilon_{em}\sigma_{bol}(T + T_{amb})(T^2 + T_{amb}^2) \quad (5)$$

where h_{con} is the convective heat transfer coefficient, ε_{em} is the effective radiation emissivity, T is the current temperature at the pipe and T_{amb} is the ambient temperature, and σ_{bol} is the Stefan-Boltzman constant. In the present study, the convective heat transfer coefficient h_{con} is assumed to be 8 W/m^2 K and the emissivity ε_{em} is set constant at 0.51 [17].

For the stainless steel surfaces, the following simplified experimental expression is used in [7]:

$$h_{stainless} = \begin{cases} 0.0668T & \left(\frac{W}{m^2\,K}\right) \quad 0 < T < 500°C \\ 0.231T - 82.1 & \left(\frac{W}{m^2\,K}\right) \quad T > 500°C \end{cases} \quad (6)$$

A FILM user subroutine is used to implement the above expressions, Eqs. (5) and (6), for the heat-transfer coefficient in ABAQUS. It is worth noting that ABAQUS allows one single user-subroutine to be written for both materials, C-Mn and SUS304, by simply specifying the surface on which each condition applies.

Due to the symmetry around the WCL, heat transfer coefficients are not applied on the plane of symmetry which in turns lead to another boundary condition on this plane. Consequently, the heat flux is zero on this plane because it is not allowed to the heat to flow out or into the symmetric plane.

The initial temperature of the entire lined pipe joint including the two welding types can be taken as a constant in space and equal to the ambient temperature, 20°C. In this case, all deactivated welding nodes keep constant, 20°C, until depositing the welding bead elements. The nodal temperature of re-birth welding elements drastically jumps to the maximum temperature as the heat source arrives by applying Eqs. (4)-(6).

However, two boundary conditions and one initial state are applied on the surfaces of lined pipe. It is observed from Fig. 2 that the radiation and convection take place from all sides of the welded lined pipe exposed to the environment except the surface at which the symmetry

plane, the WCL, is located. Furthermore, all welded lined pipe nodes have the same initial temperature, 20°C.

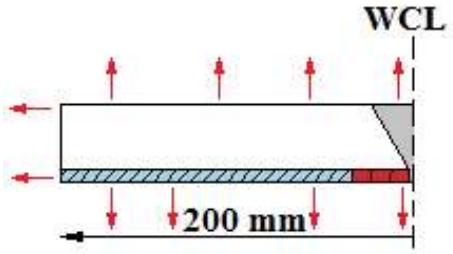

Fig.2. Effect of radiation and convection in welded lined pipe having the same initial temperature.

2.3. Mechanical analysis

The second step of the analysis depends on the thermal history of nodes which is read in ABAQUS from a results file generated during the thermal analysis. The mechanical boundary conditions are applied just to prevent rigid body motion. At the WCL, the nodes in the mechanical analysis are prevented from moving axially but they are allowed to move in any other direction in the (symmetrical) mid-plane as shown in Fig. 3.

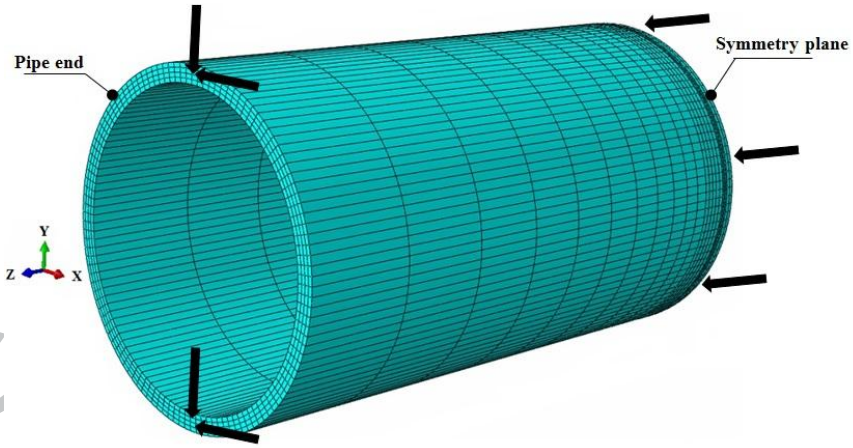

Fig. 3. Mechanical boundary conditions.

At the lined pipe end, additional degrees of freedom are restrained to restrict lateral and radial motions without affecting free expansion/contraction of the lined pipe. The automatic time step is used with a non-linear geometry effect to take into account any large deformations during welding operations.

Assuming there is no change in solid-state phase transformation in the weld and base metals, the total strain rate $\dot{\varepsilon}$ increment can be decomposed into three increments as follows [16]:

$$\dot{\varepsilon} = \dot{\varepsilon}^{e} + \dot{\varepsilon}^{p} + \dot{\varepsilon}^{t} \quad (7)$$

where $\dot{\varepsilon}^e$ is the elastic strain increment; $\dot{\varepsilon}^p$ is the plastic strain increment and $\dot{\varepsilon}^t$ is the thermal strain increment. Eq. (7) is correct only for a small plastic increment. The elastic strain is calculated using the isotropic Hook's law with respect to temperature-dependent Young's modulus and Poisson's ratio. The plastic strain is calculated using a rate-independent elastic-plastic constitutive equation with respect to the Von Mises yield surface, temperature-dependent mechanical properties and hardening law. The strain-hardening rate, H', is defined in Eq. (8) with respect to the stress increment, $d\sigma$, and the plastic strain increment, $d\dot{\varepsilon}^p$, as given below [18]:

$$H' = \frac{d\sigma}{d\dot{\varepsilon}^p} \tag{8}$$

Due to thermal loading and unloading during welding, kinematic hardening is executed. The thermal strain depends on the temperature-dependent coefficient of thermal expansion.

3. Validation

In order to validate the FE procedure for lined pipe welding, the numerical work of Karlsoon and Josefsson [4], validated experimentally by [5, 6], has been studied. Our approach has been applied to the Karlsoon and Josefsson model [4] where a single-pass butt-welded pipe made of C-Mn is used (Swedish standard steel SIS2172). The joint studied has an outer diameter of 114.3 mm and a wall thickness of 8.8 mm, with a 5.5 mm-deep V-groove for filler material. MIG (Metal Inert Gas) welding was used to fill the groove with a filler material from the outside in a single pass with a speed of 6 mm/s.

Our numerical results from thermal and mechanical analyses have been compared with the validated work of [4] where the circumferential angle is 150° from the start/stop location. The isotherms through the thickness illustrate the fact that there is a good correlation between our results and the experimental results of [4] as shown in Fig. 4(a) and (b). Furthermore, the residual stress distributions at 150° from the start/stop welding location on the inner surface along the axial direction correlate well with those obtained by the validated experiment [4].

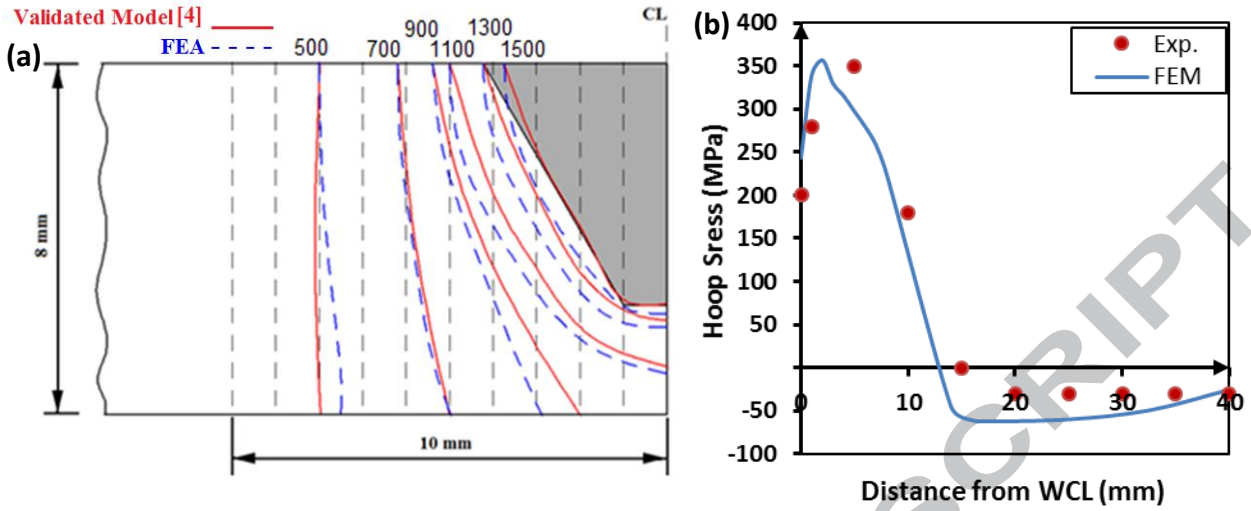

Fig. 4. Comparison of our FEA results with the experimentally validated results in [4] at θ=150°. (a) Thermal isotherms through thickness (°C) and (b) residual hoop stress distributions on the inner surface.

Similarly, in order to validate the weld overlay FEA approach, Deng and Murakawa [8] conducted welding experiments on SUS304 pipe with two-pass GTA welding. The outer diameter is 114.3 mm with a thickness of 6 mm. The thermal history findings have been numerically compared with their experimental counterparts at three axial locations at 180° central angle in Fig. 5(a). The three points 1, 2 and 3 are located at 3 mm, 8mm, and 13 mm from the FZ boundary, respectively. In addition, results for residual hoop stress taken from our FE structural model are compared in Fig. 5(b) with the experimental results in [8] at an angular location θ from the welding start/stop point of 180° on the inner surface against axial distance from the welding centreline.

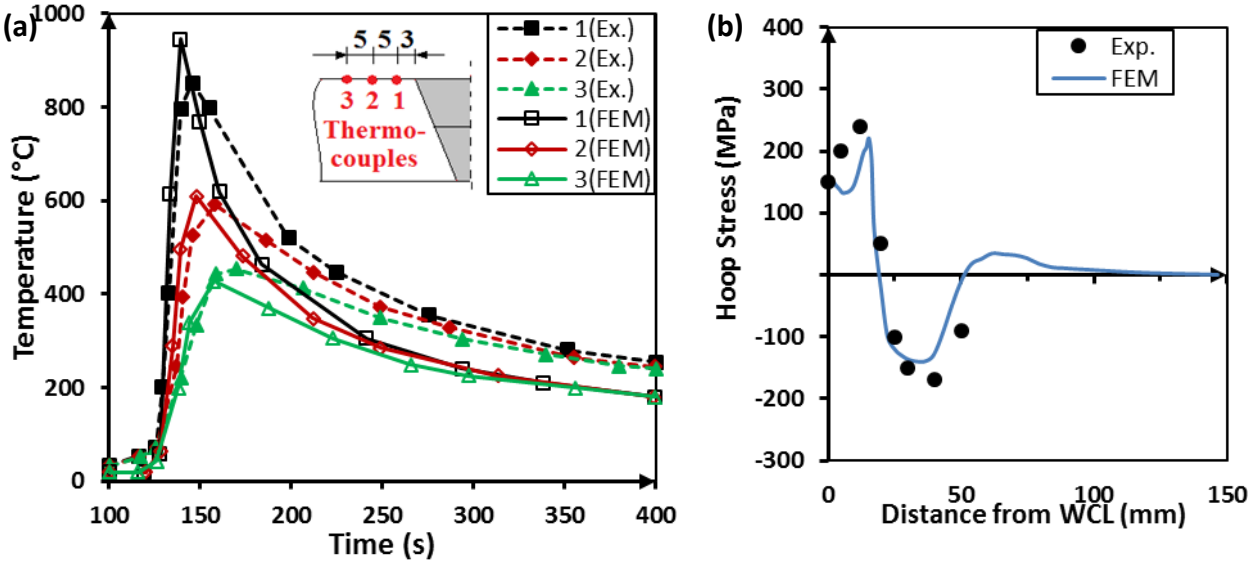

Fig. 5. Comparison of our FEA results with the experimental results in [8] at θ=180°: (a) temperature history at point

1, 2 and 3; (b) hoop residual stress distributions on the inner surface.

It can be seen from the comparisons in Figs. 3 and 4 that there is reasonable agreement between our thermal and structural FE results and the experimental results in [4] and [8]. Therefore, the FE approach applied in this study is considered suitable for simulating weld overlay and girth welding in order to produce the thermal and structural analyses for the lined pipe.

4. Description of the lined pipe segment and welding conditions

Using ABAQUS 6.13-1 [12], the thermal and mechanical FE computational procedures described in Section 2 have been implemented to calculate the transient temperature field during welding of two segments of lined pipe, in which a one-pass weld overlay and a one-pass butt-weld are implemented sequentially. The lined-pipe segment has an outer diameter of 114.3 mm and a wall thickness of 6 mm, of which 4.5 mm is the thickness of the C-Mn outer pipe and 1.5 mm is the liner thickness, as shown schematically in Fig. 6. Only one segment of the lined pipe, which is 200 mm long, is analyzed due to the symmetry about the WCL.

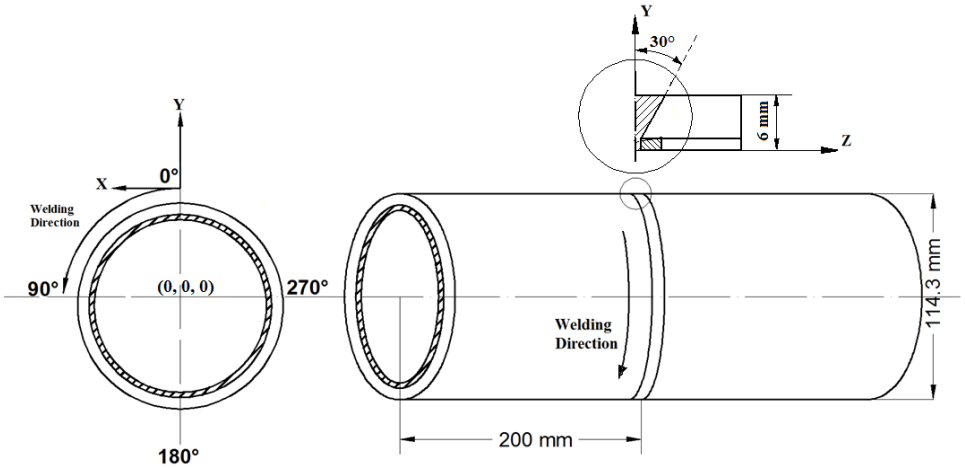

Fig. 6. Dimensions of analysis model.

The outer pipe material is carbon-manganese (C-Mn) steel with a chemical composition of 0.18%C, 1.3%Mn, 0.3% Si, 0.3%Cr, 0.4%Cu (Swedish standard steel SIS2172). The temperature-dependent thermo-mechanical material properties, namely, density, specific heat, conductivity, thermal expansion coefficient, yield stress, Young's modulus and Poisson's ratio used for the outer pipe are taken from the work of Karlsson and Josefson [4] as shown in Table 1. The thermo-mechanical properties of the SUS304 SS liner are obtained from the study of Deng and Murakawa [8] as shown in Table 2. The GTA-welding process is used in

filling the girth weld and weld overlay groove. The same thermo-mechanical material properties are used for both base and weld metals except for the yield stress, where the weld material has higher yield stress in both C-Mn steel and SUS304 SS.

Table 1. Thermo-mechanical properties of C-Mn [4].

Temperature (°C)	Density (kg/m^3)	Specific heat (J/kg K)	Conductivity (W/m K)	Thermal expansion (x10^{-5} K^{-1})	Yield stress (MPa)		Young's modulus (GPa)	Poisson's ratio
					Base	Weld		
0	7860	444	50	1.28	349	445	210	0.26
100		480	48.5	1.28	331	441	200	0.28
200		503	47.5	1.30	308	416	200	0.29
300		518	45	1.36	275	376	200	0.31
400		555	40	1.40	233	326	170	0.32
600		592	35	1.52	119	173	56	0.36
800		695	27.5	1.56	60	43	30	0.41
1000		700	27	1.56	13.00	14	10	0.42
1200		700	27.5	1.56	8.00	9	10	0.42
1400		700	35	1.56	8.00	9	10	0.42
1600		700	122.5	1.56	8.00	9	10	0.42

Table 2. Thermo-mechanical properties of SUS304 [8]

Temperature (°C)	Density (kg/m^3)	Specific heat (J/kg K)	Conductivity (W/m K)	Thermal expansion (x10^{-5} K^{-1})	Yield stress (MPa)		Young's modulus (GPa)	Poisson's ratio
					Base	Weld		
0	7900	462	14.6	1.70	265	438	199	0.294
100	7880	496	15.1	1.74	218	402	193	0.295
200	7830	512	16.1	1.80	186	382	185	0.301
300	7790	525	17.9	1.86	170	362	176	0.310
400	7750	540	18.0	1.91	155	346	167	0.318
600	7660	577	20.8	1.96	149	256	159	0.326
800	7560	604	23.9	2.02	91	97	151	0.333
1200	7370	676	32.2	2.07	25	28	60	0.339
1300	7320	692	33.7	2.11	21	16	20	0.342
1500	7320	700	120	2.16	10	12	10	0.388

In this research, a linear kinematic hardening law using the Von Mises criterion has been assumed for C-Mn and SUS304 with a bilinear stress-strain curve. Fig. 7 illustrates the temperature-dependent yield stress as the plastic strain of SUS304 and C-Mn is equal to 1% [18, 19].

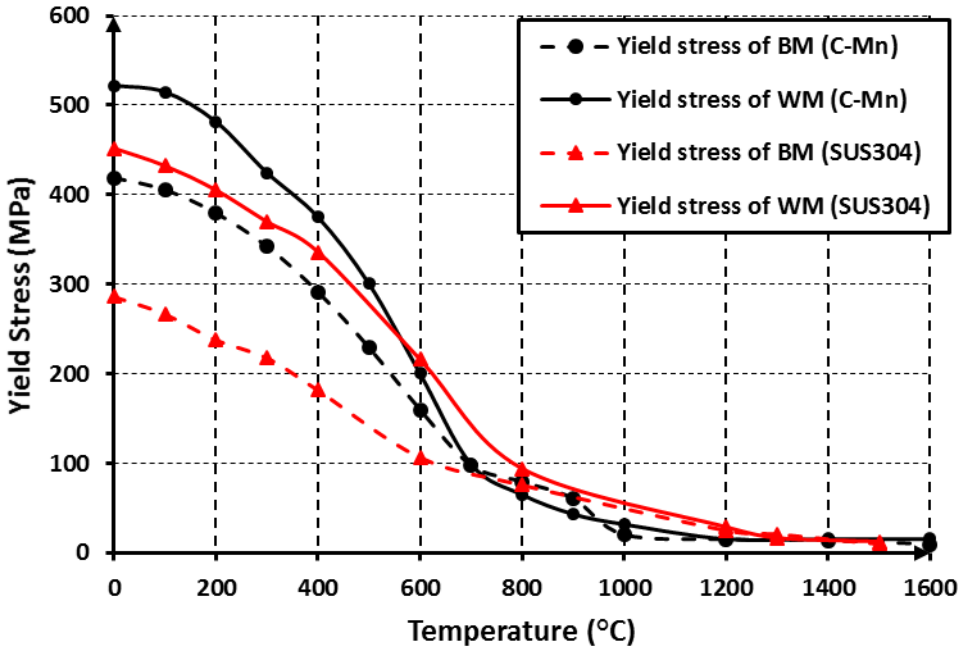

Fig. 7. Yield strength of SUS304 [18] and C-Mn steel [19] corresponding to 1% hardening.

The numerical values for the variables in the power density distribution in Eq. 4 are illustrated in Table 3 for each welding material.

Table 3. Heat source and welding parameters.

		SUS304	C-Mn
Half-length of arc (mm)	a	2.765	3.26 mm
Depth of arc (mm)	b	2.575	3.2 mm
Half-width of arc (mm)	c	1.5 mm	3 mm
Welding current (A)	I	8	20
Voltage (V)	V	120	170
Welding speed (mm/s)	v	1.33	6.25 mm/s
Welding efficiency	μ	70%; Gas Tungsten Arc (GTA) [15]	85%; Metal Inert Gas (MIG)[15]

Based on the heat torch parameters presented in Table 2, the power density distributions of a Goldak ellipsoidal heat source along the welding directions for SUS304 and C-Mn are depicted in Fig. 8.

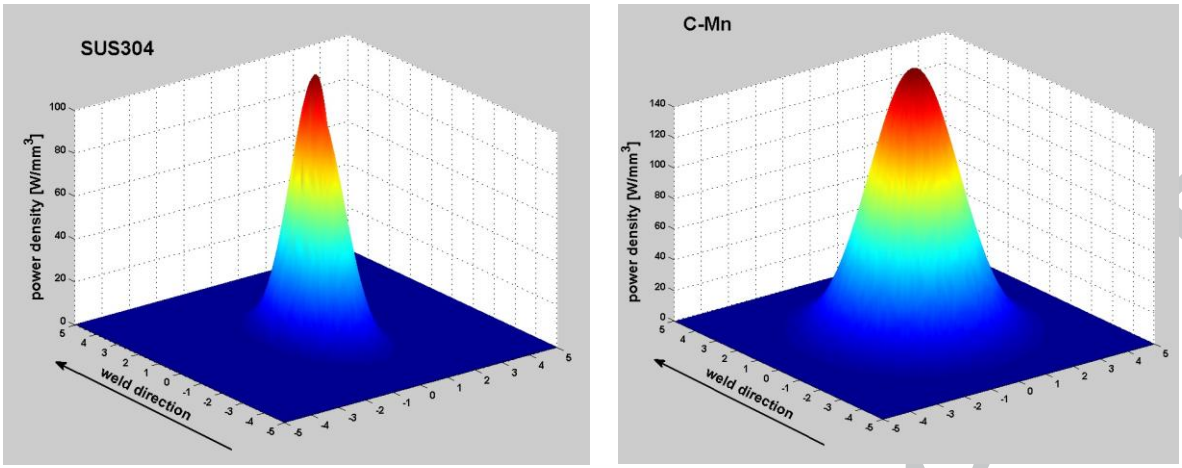

Fig. 8. Power density distributions of Goldak ellipsoidal heat source models, C-Mn and SUS304.

The latent heat for C-Mn steel is set to be 247kJ/kg between the solidus temperature of 1440 °C and the liquidus temperature of 1560 °C. For stainless steel (SUS304), the latent heat is assumed to be 260kJ/kg between 1340 °C and 1390 °C solidus and liquidus temperatures, respectively. Consequently, the melting point for C-Mn is 1500 °C and 1365 °C for SUS304. The initial temperature of the lined pipe and the weld bead is set at room temperature.

5. Simulation results from thermal analysis

Based on our welding procedure, we assume that the typical welding model entails three conditions. Firstly, all nodes in the FZ should reach at least the melting temperatures of C-Mn or SUS304, which are 1500°C and 1365°C, respectively, to guarantee sufficient fluidity for the material to be deposited properly into the weld grooves. Secondly, the peak temperatures at the WCL nodes should be identical as long as the welding parameters such as the net heat input and welding pool geometry are kept constant. Finally, the extent of HAZ should be 2-3 mm from the FZ boundary where the net heat input plays an important role in specifying this distance. In this case, the assumed HAZ receives peak temperatures ranging between the melting point and 800-900°C [7].

In the present study, the thermal history profiles are obtained at six locations along the axial direction for Case A, Case B and Case C where points T1, T2 and T3 are placed upon the inner surface while points T4, T5 and T6 are mounted on the outer surface as shown schematically in Fig. 9.

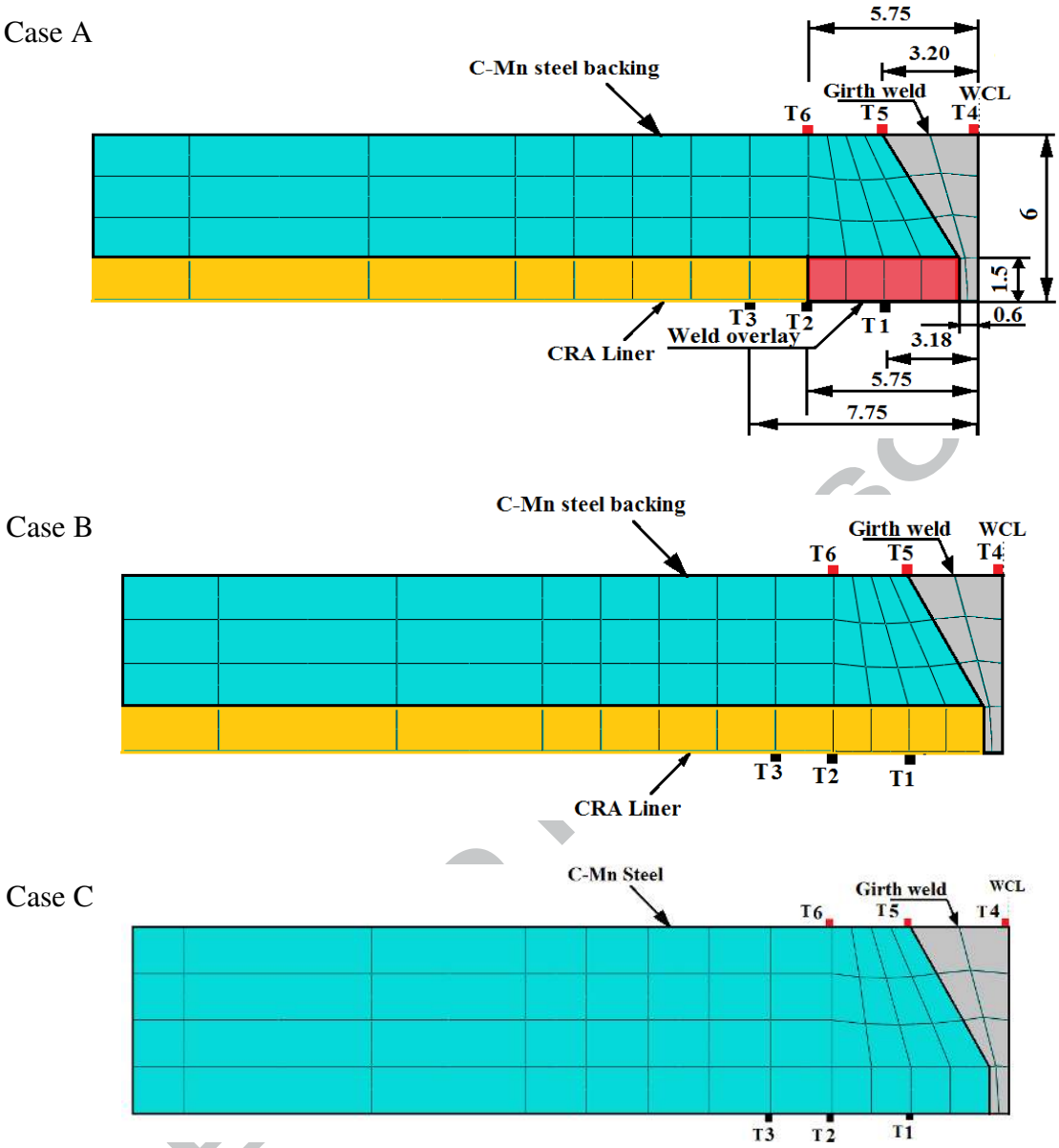

Fig. 9. Schematic sketch of predicted temperature positions in Case A, Case B and Case C along the axial direction (mm).

5.1. Temperature fields induced by weld overlay and girth welding (Case A)

In this paper, Case A is considered a reference case in which the effect of the weld overlay operation and the existence of a liner as protector of the C-Mn steel backing are examined.

In Case A, the distribution at point T1 reaches a maximum peak temperature of 2084°C as a balance between the flux and the heat losses. It can be seen that the peak temperature stays on the point for an instant since the heat source moves with a constant velocity. Once the heat source has passed point T1, a rapid drop in the temperature occurs, as shown in Fig. 10.

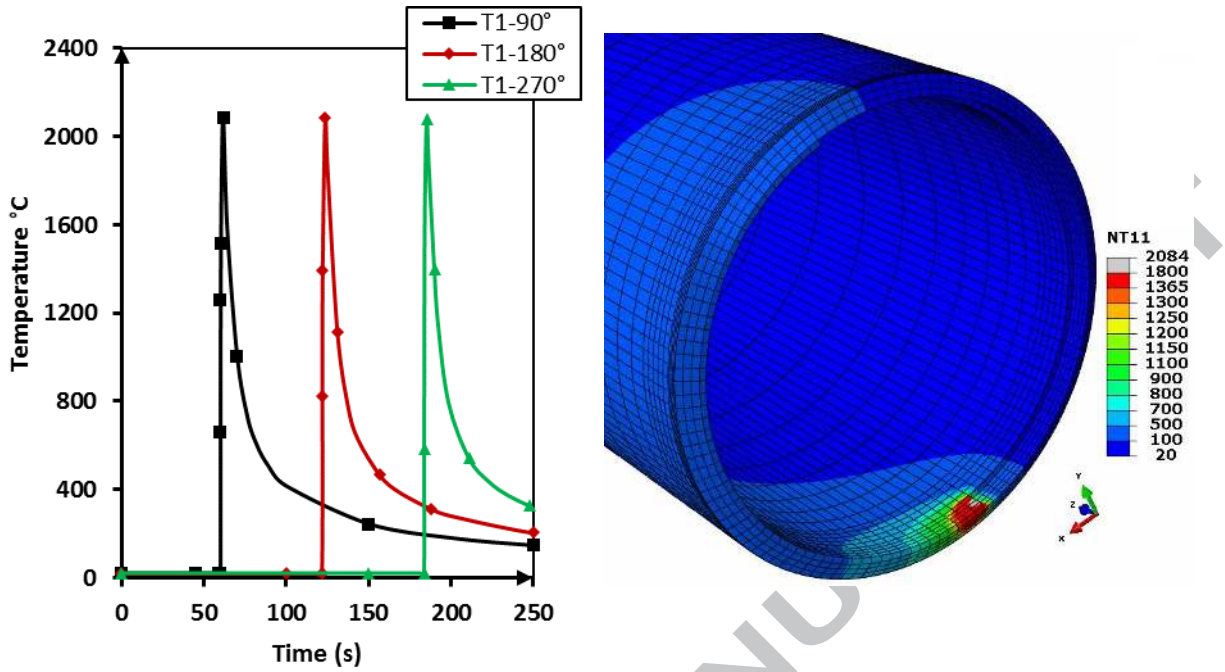

Fig. 10. Temperature histories during weld overlay on point 1 at different central angle 90°,180° and 270°.

The thermal history of point T4 located at the outer surface of C-Mn backing steel is illustrated in Fig. 11. Point T4 is placed on the WCL of the girth welding where the heat source is applied. Consequently, the temperature reaches a maximum of 2430°C.

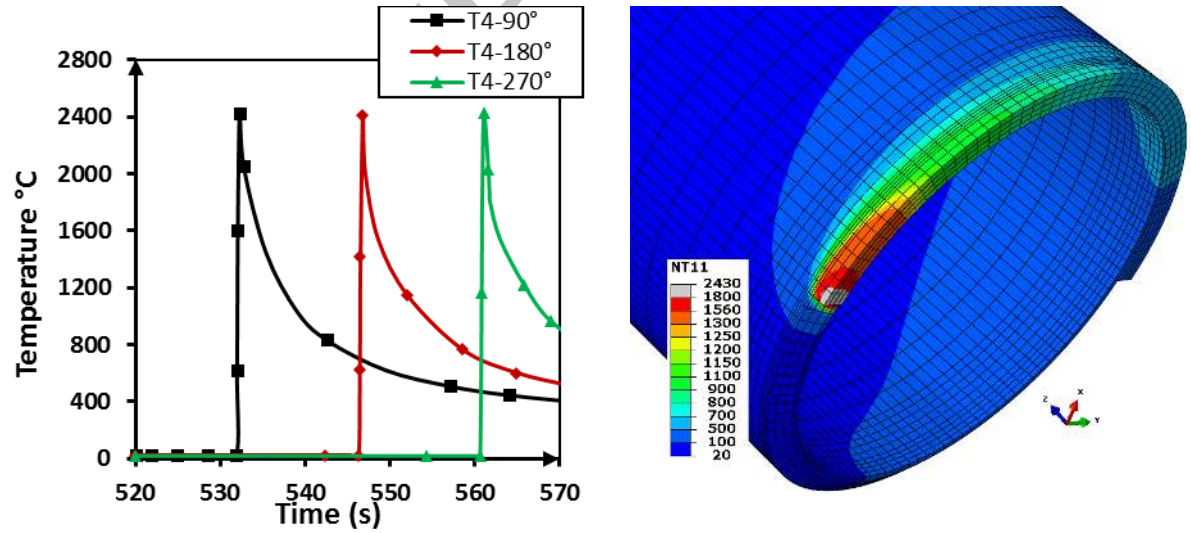

Fig. 11. Temperature histories during girth welding at point T4 (WCL) at different central angles 90°,180° and 270°.

The thermal history and peak temperatures obtained at points T1 and T4 at three different circumferential angles 90°, 180° and 270° from the start/stop position during weld overlay and girth welding are clearly identical as illustrated in Figs. 10 and 11, respectively. As a result, circumferential angle has a negligible effect on the temperature history.

Fig. 12 illustrates the temperature histories at six points during the time span of weld overlay and girth welding with considerable cooling time between them. Once the overlay weld is finished, the whole lined pipe cools down for 270 seconds to reduce the maximum pipe temperature to around 100°C, which is called the inter-pass temperature [8]. From the thermal results depicted in Fig. 12, it is clear that our FE welding approach for both welds have satisfied the three conditions of a typical welding mentioned earlier in Section 5.

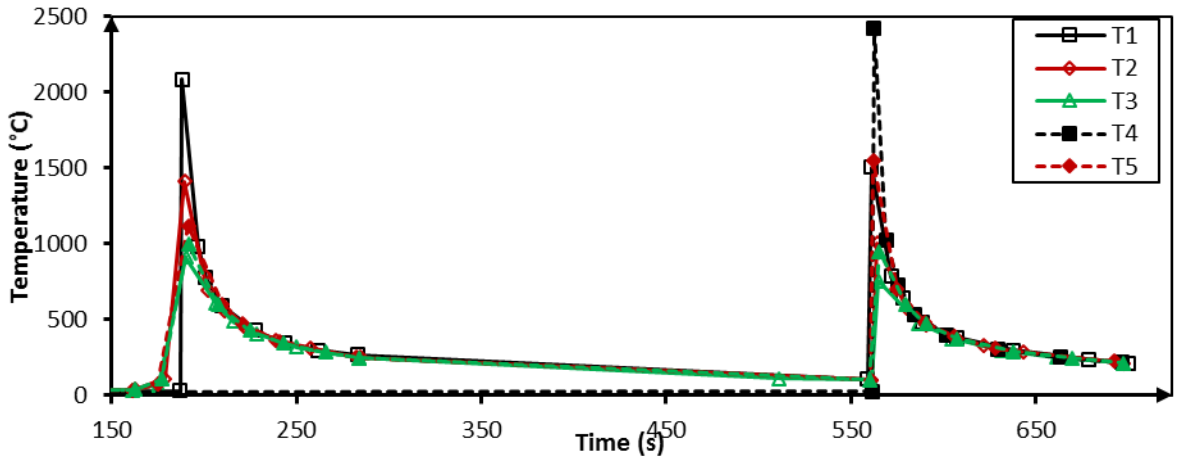

Fig. 12. Temperature history for points T1-T6 at 180° from the welding start/stop location with 270 s interval time (248-518 s) in Case A.

5.2. Temperature fields induced by girth welding without weld overlay (Case B)

In this work, the focus of attention is on the effect of the weld overlay on the thermal and mechanical results. In case B, the liner is fixed underneath the C-Mn steel but the weld overlay is not simulated in the FE model.

For case B, the welding temperatures are taken from 6 points at 180° where points T1, T2 and T3 are on the inner surface and points T4, T5 and T6 are on the outer surface, as shown in Fig. 13.

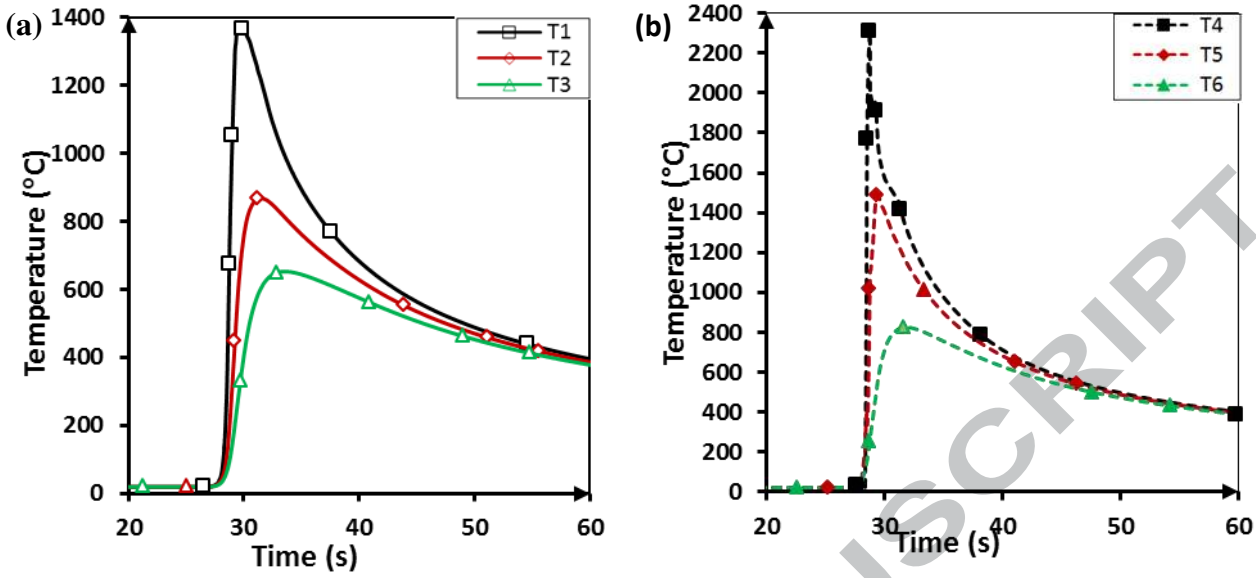

Fig. 13. Temperature history at 180° at points (a) T1, T2 and T3, on inner surface and (b) T4, T5, and T6 on outer surface in case B.

The maximum temperatures on points T1, T2 and T3 are 1366°C, 868°C and 651°C, respectively. On the other surface, the peak temperatures at points T4, T5 and T6 are 2310°C, 1485°C and 821°C, respectively. In comparison with the results of Case A, it is clear that there is a significant difference, particularly on the inner surface where Case A results are much larger than their counterparts in Case B.

The disparity between the results of cases A and B becomes larger as the distance from the WCL decreases.

On the outer surface, the maximum temperature at point T4 in Case A is higher by 110°C than its counterpart in Case B. This difference is explained by the inter-pass temperature in Case A which is not present in Case B. In both cases, it is worth noting that the decrease of the maximum temperature along the axial direction has a nonlinear trend [14]. The reason is attributed to the nonlinear heat input of the heat source and the nonlinearity of material thermal properties in terms of temperature.

5.3. Temperature field induced by girth welding without liner (Case C)

In contrast to Case A and Case B, there is no liner protecting the C-Mn steel in Case C but the total thickness is still the same as the previous cases, 6 mm. Hence, the material of the whole pipe is C-Mn steel. Furthermore, the heat transfer coefficient used in this case is that solely assigned to the carbon steel material as given in Eq. (5). Fig. 14 plots the temperature versus time for Case C at points T1, T2, T3, T4, T5 and 6 where the circumferential angle is

180°. The peak temperatures at these points are 1310°C, 793°C, 622°C, 2303°C, 1474°C, and 807°C, respectively. It is obvious from Fig. 14(a) that there is somewhat of a reduction in the maximum temperatures as per their counterparts in Case B on the inner surface. The reason is the cooling rate of C-Mn steel which is higher than that of SUS304. In other words, the heat transfer coefficient and thermal conductivity of C-Mn are much higher than that for stainless steel. In comparison with case B, the ultimate temperatures at points T4, T5 and T6 on the outer surface are identical as illustrated in Fig. 14(b) because the thermal conditions, namely the net heat input and the welding pool geometry, remain constant.

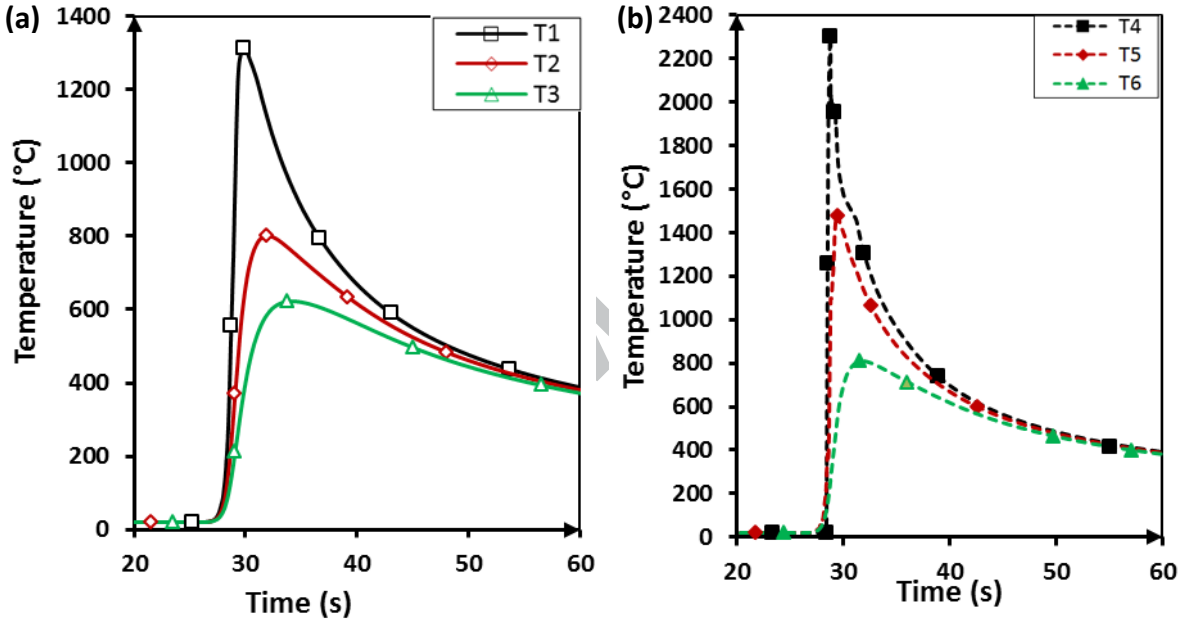

Fig. 14. Temperature history at 180° on points (a)T1, T2 and T3, inner surface and (b) T4, T5, and T6 on outer surface; case C.

6. Results from mechanical analysis

6.1. Residual stresses predicted for lined pipe (Case A)

Next, results are presented from the investigation of residual stress distributions induced by the lined pipe welding operations including weld overlay and girth welding. Variations of the residual stresses on inner and outer surfaces at three circumferential positions are shown in Fig. 15(a)-(d) as a function of axial position.

Fig. 15(a) compares the final residual stresses on the inner surface for circumferential angles from the welding start/stop position of 90°, 180° and 270°. It is worth noticing that within the FZ and its vicinity the axial residual stresses are tensile. The residual stresses have similar distributions with a maximum value at the WCL of approximately 520 MPa. According to the

FE results, when the distance from the WCL is less than 11.75 mm, the magnitude of axial residual stresses on the inner surface (liner) is higher than 269.3 MPa and this value is greater than the yield strength of SUS304 SS at room temperature. The residual stresses are tensile when the distance from the WCL is less than 34.36 mm while slightly compressive beyond this limit.

The axial residual stress results obtained by the 3-D FE model on the outer surface, C-Mn backing steel, are plotted in Fig. 15(b). The distributions are almost a mirror image of those shown in Fig. 15(a). The residual stresses are compressive from the WCL to 21 mm along the axial direction with a peak compressive residual stress on the WCL of about-496 MPa.

According to the preceding comparisons, it can be inferred that within and near the FZ the axial residual stress distributions which act normal to the weld line are compressive on the outer surface and tensile on the inner surface. The heat deposited during the weld overlay and girth welding is relatively high, enough to cause an increase in temperatures at the weld regions throughout the lined pipe thickness. Therefore, plastic deformation is produced in the whole cross-section of lined pipe in the weld overlay and girth welding zones and their vicinities. As the pipe finally cools down to room temperature, the only deformation that will generate thermal stresses during the cooling period is the bending moment because of the radial expansion and subsequent contraction. Radial shrinkage produces a tourniquet effect which is a local inward deformation in the FZ and HAZ. In other words, the axial stresses for such thin lined pipes cause a simple linear bending.

This behaviour is in line with the nature of welding as it produces tensile stresses on the liner and compressive stresses on the backing steel surface. However, the two stresses balance each other [8].

In our case, the axial shrinkage induced by the girth welding is not resisted by the earlier weld overlay because the inside surface near the girth welding zone can reach over 1300°C as the girth welding is conducted. Basically, the yield stress plays a vital role in determining the axial residual stresses because the yield stress of girth welding filler material is higher than that of SUS304 welding material for lower temperatures. Consequently, the tensile axial residual stress at the WCL in the inner surface is 520 MPa whereas it is 269.3 MPa at the HAZ of the liner. Moreover, in C-Mn steel, the yield stress of the base material is lower than the yield stress of the girth welding filler material. As a result, the axial residual stress at the WCL, -496 MPa, is higher than that at the HAZ on the outside surface. Away from the FZ

and HAZ, the tensile axial residual stress turns into compressive stress on the inside surface and vice versa on the outside surface. Through careful observation of Fig. 15(a) and (b), it can be clearly seen that the axial stress distributions around the welding direction have an almost homogenous distribution on the outer and inner surfaces. Consequently, the axial residual stress distributions do not strongly depend on the angular position [11].

Turning to the hoop stress which is defined as the stress acting parallel to the WCL, Fig. 15(c) portrays the hoop residual stress results on the inner surface for the three central angles. Unlike Fig. 15(a) at the WCL, equilibrium considerations require that the tensile hoop stresses at the FZ of girth welding are relatively lower than those in the HAZ for SUS304 material.

Fig. 15(d) represents the hoop residual stresses on the outer surface with 90°, 180° and 270° central angles. The numerical results show that there are compressive hoop stresses at the FZ and its vicinity. At the region, $Z \leq 50$ mm in the FZ and its adjacent area, it can be observed that the residual hoop stress distributions have a wavy form.

The residual stress distributions obtained from the simulation of the welded lined pipe show a very complex shape with respect to the axial direction from the WCL.

With regard to the hoop residual stress distributions in Fig. 15(c) and (d), their magnitudes are affected by the axial residual stresses; the hoop residual stresses are tensile on the inner surface at the FZ and the area adjacent to it. For the self-equilibrating purpose, stress reversal from compressive to tensile and vice versa is noticed on the outer and inner surfaces away from the WCL, respectively.

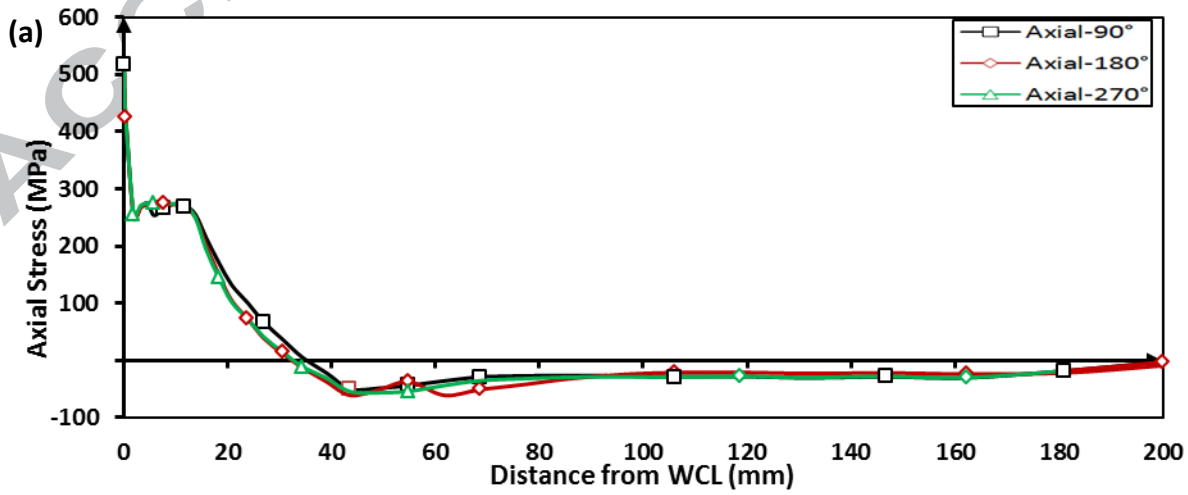

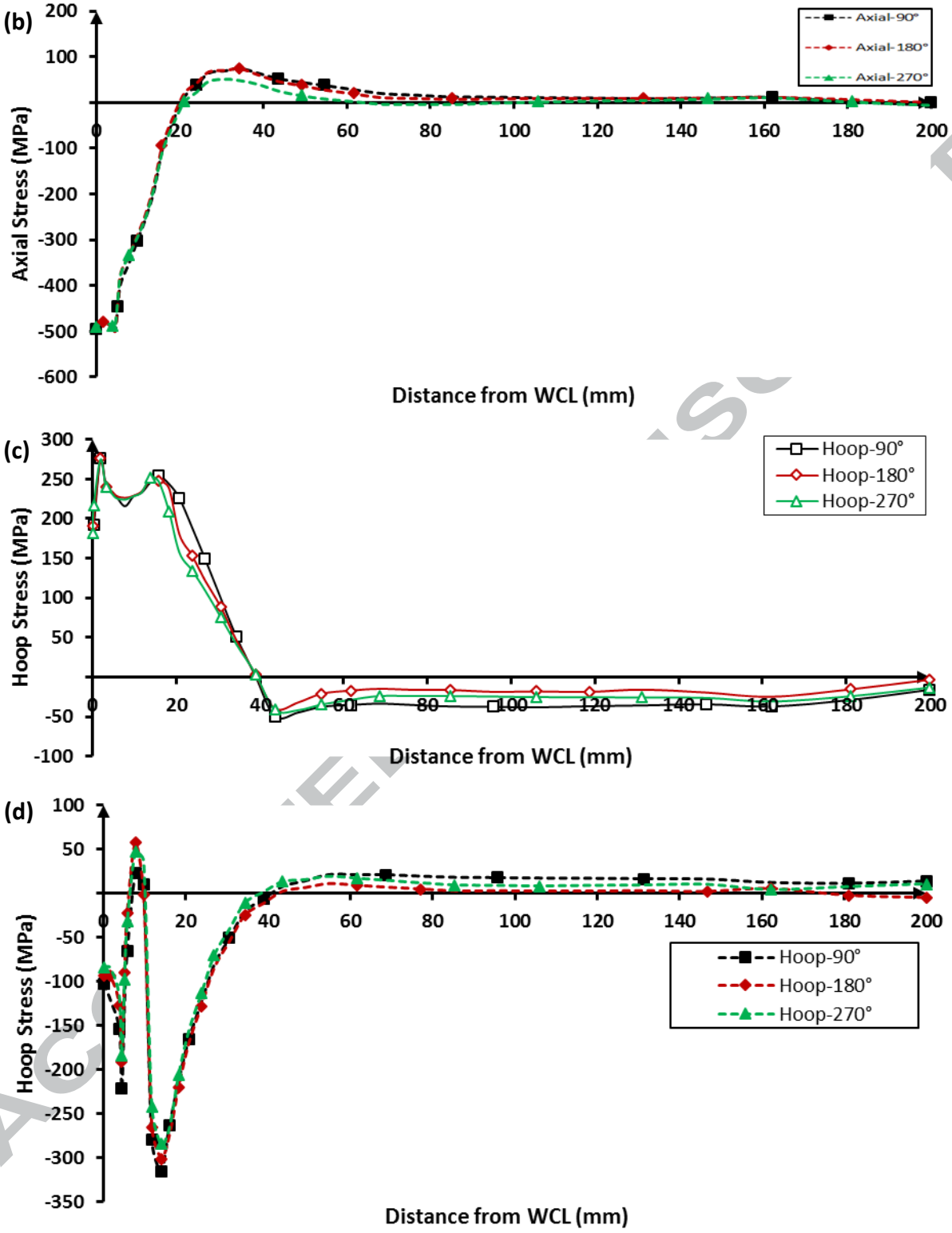

Fig. 15. Residual stress distributions in Case A at different central angles 90°, 180° and 270°: (a) axial stress distributions on the inner surface (SUS304), (b) axial stress distributions on the outer surface (C-Mn), (c) hoop stress distributions on the inner surface (SUS304), and (d) hoop stress distributions on the outer surface (C-Mn).

At the 0°/360° central angle, there is an overlapping of the heat source which influences the final hoop and axial residual stresses. However, at circumferential angles greater than 0°,

there is no overlapping and hence the final residual stresses are not changed by changing the circumferential angle as illustrated in Fig. 16 which shows von Mises stress results.

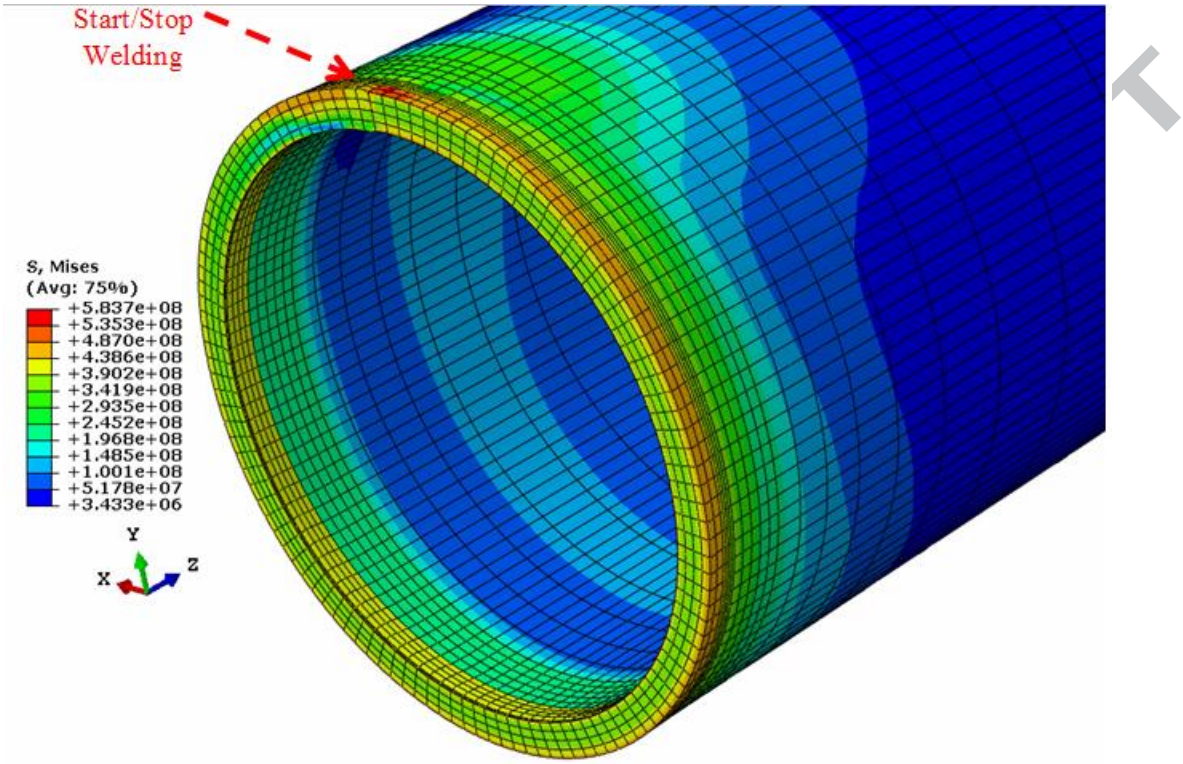

Fig. 16. Von Mises residual stress distributions around the welded lined pipe.

6.2. Mechanical deformations

For a pipe, in general, the radial deformations are of special interest. Fig. 17 compares numerical results for radial displacement at the cross-section of 180° central angle on the inner surface resulting from welding in Case A, Case B and Case C. These results are taken after cooling the entire lined pipe to an ambient temperature. The residual state in this section shows negative radial displacements in the three cases (more in the weld regions). However, this is mainly an effect of the global deformation pattern as indicated by the displacement along the axial direction. Fig. 17 may help to emphasise this global deformation pattern. Note that the elements representing the weld overlay and girth welding are not deformed as large as the displacement plot illustrates [4]. In particular, the initial configurations (stress and strain-free) of these elements are those determined by the positions of the nodes at the time of bead deposition.

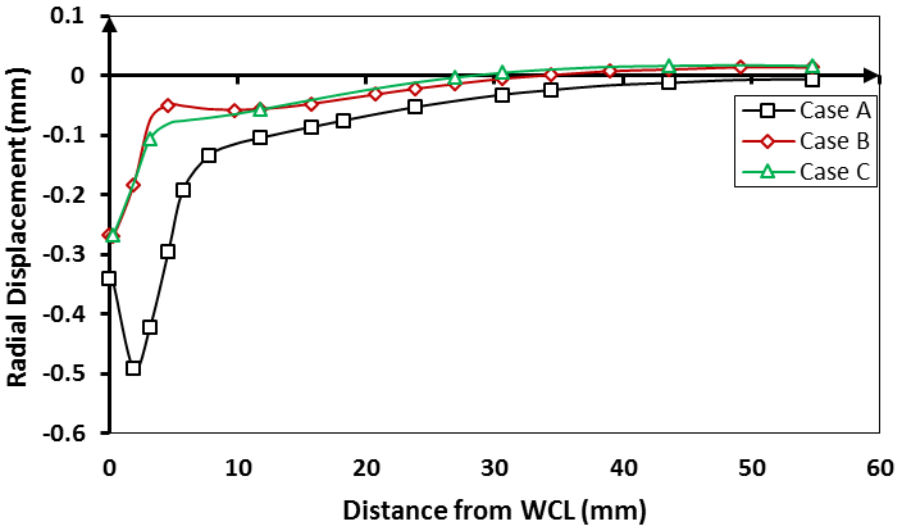

Fig. 17. Radial displacements of inner surface at 180° central angle

The maximum radial shrinkage, 0.5 mm, at a distance of 1.9 mm from the WCL, is obtained in Case A. This is attributed to the effect of two welds at 1.9 mm on the inner surface, i.e. weld overlay and girth welding. However, the HAZ of the girth welding at the inner surface is itself the FZ during the weld overlay. As a result, this region accumulates higher effective plastic strains at a typical radial positon. The extent of the region which is affected by the negative residual radial displacement is 50, 34 and 28 mm in Case A, Case B and Case C, respectively.

6.3. Influence of weld overlay and liner on residual stresses

In order to clarify the influence of using liners and weld overlay on the residual stresses, Fig. 18(a)-(d) compares the axial and hoop stress results on the inner and outer surfaces with a 180° central angle within Case A (basic case), Case B (without weld overlay) and Case C (without liner).

The peak values of the axial residual stresses on the inner surface at the WCL are 520, 434 and 312 MPa in the three cases as depicted in Fig. 18(a). Temperatures in Case A and B are higher than those in case C at the FZ. The main reason is attributed to the same filler material in the FZ of girth welding which has the same conductivity and coefficient of thermal expansion. As a result, the higher the temperature, the higher will be the axial residual stress due to a wide range of first expansion and subsequent contraction. In the HAZ, the maximum values go to Case C instead of Case A and Case B. The C-Mn steel has a higher yield stress than that of SUS304. Thus, the higher the yield stress, the higher will be the axial residual stress.

Fig. 18(b) shows the axial residual stress distributions predicted on the outer surface in Case A, Case B and Case C. We can see that the discrepancies in the compressive axial stresses among the three cases are very small in the FZ and HAZ where Case A has slightly higher compressive stresses than the others. Beyond these zones, the curves become closer to each other reflecting the convergence of temperatures along the axial direction on the outer surface for the three cases.

Fig. 18(c) compares the hoop stresses on the inner surface observed in the three cases at 180° central angle. Residual hoop stresses are highly important in cylinders and axial residual stresses in the FZ and HAZ which are tensile and compressive on the inner and outer surfaces, respectively, play a significant role in determining the magnitudes of hoop residual stresses especially in these zones In other words, the hoop stresses on the inner surface are more tensile than their counterparts on the outer surface in the FZ and HAZ. At the area away from the FZ and its vicinity, the hoop residual stresses agree reasonably with the axial residual stresses.

Fig. 18(d) compares the residual hoop stresses on the outer surface for the three cases. It can be seen that the hoop stress distribution expected in Case C at the FZ and its adjacent area ($Z \leq 50$ mm) has lower compressive stresses and larger tensile stresses than the other two cases. Beyond this axial range, the hoop stress distributions are almost identical in the three cases. The results estimated in Case A are much closer to those estimated in Case B. The simulation results also show that the residual hoop stress distributions on the outer surface have a wavy form in the FZ and its adjacent area [20].

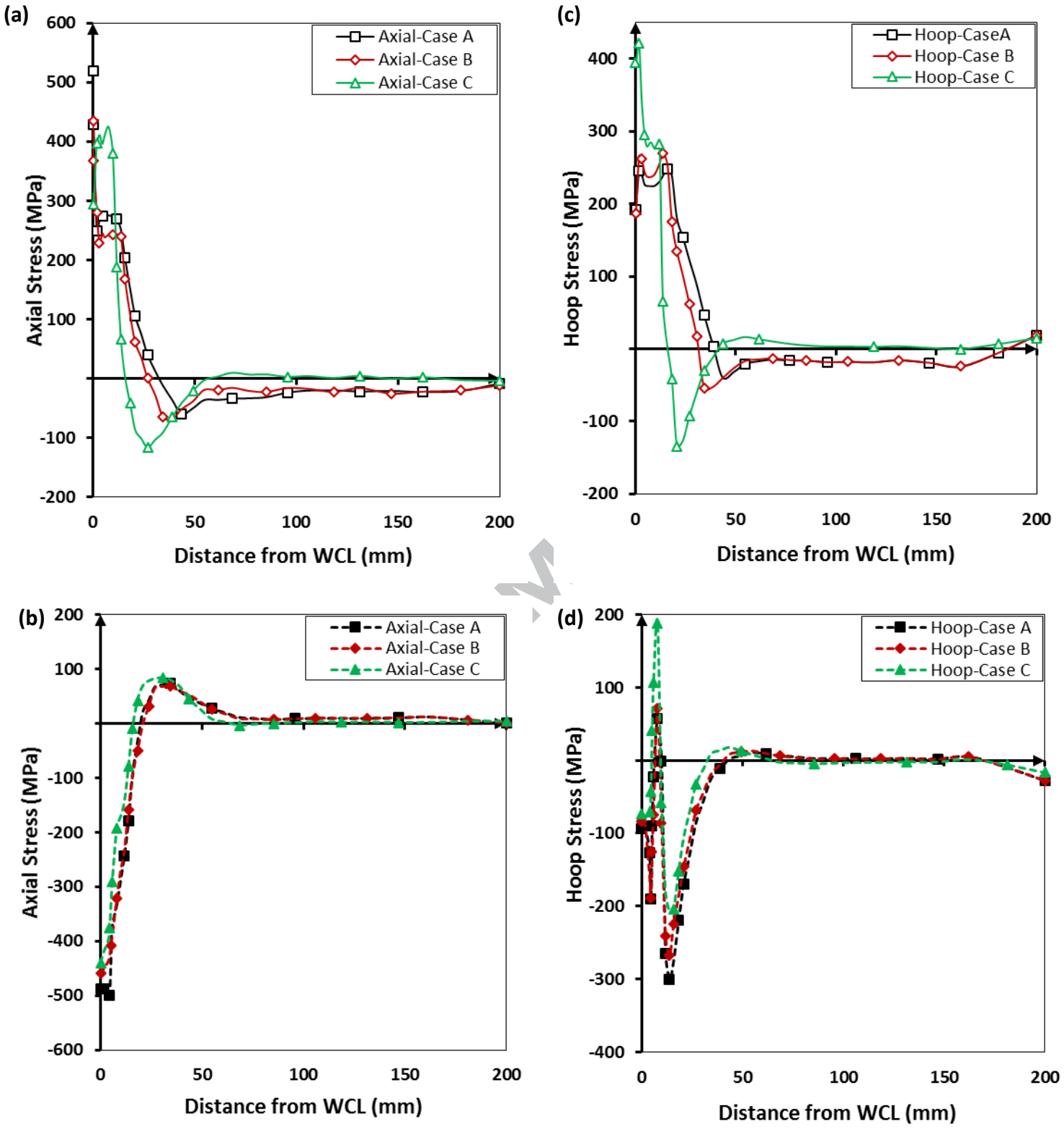

Fig. 18. Comparison of residual stresses at 180° central angle for Case A, Case B and Case C: (a) axial stress distributions on the inner surface, (b) axial stress distributions on the outer surface, (c) hoop stress distributions on the inner surface, and (d) hoop stress distributions on the outer surface.

Fig. 18(a)-(d) demonstrates that the three cases have similar trends in hoop and axial residual stress distributions especially at the outer surface. In general, the variations in outcomes among the three cases arise from the differences in the coefficient of thermal expansion, yield stress, heat transfer coefficient and thermal conductivity.

High yield stress and coefficient of thermal expansion result in higher residual stresses. Furthermore, a high coefficient of thermal expansion in conjunction with a high heat transfer coefficient and low thermal conductivity stretches the region of tensile stress adjacent to the FZ along the axial direction on the inner surface.

7. Conclusions

This paper presents a 3-D FE model executed by using ABAQUS 6.13-1 to generate temperature fields and residual stresses induced by two circumferential welds, namely, weld overlay and girth welding, in Case A. Each weld is made with different materials – stainless steel and carbon steel which are suitable for their base materials. Based on FORTRAN codes, two user-subroutines have been developed to represent the distribution of power density of the moving heat source and the non-linear heat transfer coefficients for C-Mn and SUS304. The effects of radiation and convection have been taken into account. Furthermore, the FE model procedure has been validated thermally and mechanically against experimental results reported in the literature for similar material butt-welded pipes. Moreover, the thermal history and residual stresses have been examined without considering weld overlay, described as Case B, and without liner, described as Case C, and compared with Case A. According to the simulation results in this work, the following conclusions can be drawn:

(1) Based on the thermal and mechanical results, it is clear that the temperature and residual stress distributions along the axial direction reach a steady state when the welding torch moves to fill the weld overlay and the girth welding. From the outcome of our investigation it is possible to conclude that the thermal history and residual stresses are not sensitive to the variations of the circumferential angles, except for the heating area around the start/stop location because of the heat source overlap.

(2) Keeping the net heat input and other welding parameters constant, the maximum temperature at the WCL in Case A, the reference case, is slightly higher because the inter-pass temperature is higher than its counterparts on the outer surface in Case B, with using the liner but without considering the weld overlay, and Case C, without considering the liner and weld overlay. On the inner surface, the temperature results

along the axial direction in Cases A and B are higher than those in Case C because the cooling rate of C-Mn is higher than that of the SUS304.

(3) Corresponding to the residual stress results, the residual stress distributions have a slightly similar trend in the three cases. The axial residual stress distributions on the inner surface and the outer surface have a converse trend. In the FZ and HAZ, tensile axial residual stresses are produced on the inner surface whilst compressive axial stresses are generated on the outer surface. Away from the FZ and HAZ, compressive axial stresses are formed on the inner surface whereas tensile axial stresses are produced on the outer surface. The hoop stresses have the same distribution trend as the axial stress on the inner surface but the magnitude of the tensile stress at the WCL is much smaller. On the outer surface, the wavy form of hoop stress distributions depend on the distance from the WCL.

(4) The largest radial shrinkage in Case B and Case C occurs at the WCL, whilst it takes place at the center of weld overlay in Case A with higher values in Cases B and C. The radial contraction gradually reduces towards the ends of the lined pipe.

(5) Comparing the three cases, we have established that the axial residual stresses at the FZ on the inner surface are affected by the maximum temperature where higher temperatures produce higher levels of axial residual stress. There is no distinctive variation among the axial residual stresses on the outer surface because of the same welding and base materials. Considering the equilibrium on the inner surface, the axial residual stresses play a key role in determining the hoop residual stresses in FZ and its vicinity. Moreover, the axial residual tensile stresses at the weld root are important due to the fatigue crack initiation at this point. Therefore, it is more practical to put more focus on the axial residual stresses. The hoop residual stress distributions on the outer surface have a similar wavy form to some extent.

In this work, the thermo-mechanical evolution induced by a single-pass weld overlay and girth welding have been discussed. However, the promising findings of thermo-mechanical analysis presented here for typical lined pipe welding suggest that this approach can also be useful for multi-pass weld overlay and girth welding. Moreover, work on the experimental verification of multi-pass welds in lined pipe is in progress and will be presented in a forthcoming paper.

Acknowledgments

The first author wishes to gratefully acknowledge the financial support provided by Al-Baath University and the British Council.

References

[1] Fu, A.Q., Kuang, X.R., Han, Y., Lu, C.H., Bai, Z.Q., Yin, C.X., Miao, J., Feng, Y.R., Wei, Y.G., Tang, Q. and Yang, Y., 2016. Failure analysis of girth weld cracking of mechanically lined pipe used in gasfield gathering system. *Engineering Failure Analysis*, 68, pp.64-75. doi:10.1016/j.engfailanal.2016.05.034

[2] De Koning, A. C., & Nakasugi, H. (2004). Li Ping (2004),"TFP and TFT Back in Town (Tight Fit CRA Lined Pipe and Tubing)". *Stainless Steel World*, 53-61.

[3] Bate, S. and Smith, M., 2016. Determination of residual stresses in welded components by finite element analysis. Materials Science and Technology, 32(14), pp.1505-1516. doi:10.1080/02670836.2016.1209882

[4] Karlsson, R. I., & Josefson, B. L. (1990). Three-dimensional finite element analysis of temperatures and stresses in a single-pass butt-welded pipe. *Journal of pressure vessel technology*, *112*(1), 76-84. doi:10.1115/1.2928591

[5] Jonsson, M., & Josefson, B. L. (1988). Experimentally determined transient and residual stresses in a butt-welded pipe. *The Journal of Strain Analysis for Engineering Design*, *23*(1), 25-31. doi:10.1243/03093247V231025

[6] Karlsson, C. T. (1989). Finite element analysis of temperatures and stresses in a single-pass butt-welded pipe-influence of mesh density and material modelling. Engineering computations, 6(2), 133-141. doi:10.1108/eb023767

[7] Brickstad, B., & Josefson, B. L. (1998). A parametric study of residual stresses in multi-pass butt-welded stainless steel pipes. *International Journal of Pressure Vessels and Piping*, *75*(1), 11-25. doi:10.1016/S0308-0161(97)00117-8

[8] Deng, D. and Murakawa, H. (2006). 'Numerical simulation of temperature field and residual stress in multi-pass welds in stainless steel pipe and comparison with experimental measurements', *Computational materials science,* 37(3), pp. 269-277. doi:10.1016/j.commatsci.2005.07.007

[9] Akbari, D., & Sattari-Far, I. (2009). Effect of the welding heat input on residual stresses in butt-welds of dissimilar pipe joints. *International journal of pressure vessels and piping*, *86*(11), 769-776. doi:10.1016/j.ijpvp.2009.07.005

[10] Deng, D., Kiyoshima, S., Ogawa, K., Yanagida, N., & Saito, K. (2011). Predicting welding residual stresses in a dissimilar metal girth welded pipe using 3D finite element model with a simplified heat source. *Nuclear Engineering and Design*, *241*(1), 46-54. doi:10.1016/j.nucengdes.2010.11.010

[11] Obeid, O., Alfano, G. and Bahai, H., 2017. Thermo-Mechanical Analysis of a Single-Pass Weld Overlay and Girth Welding in Lined Pipe. Journal of Materials Engineering and Performance, pp.1-16. doi:10.1007/s11665-017-2821-5

[12] ABAQUS Documentation, release 14. Dassault Syste`mes, Providence,RI.

[13] Deng, D., Zhang, C., Pu, X. and Liang, W., 2017. Influence of Material Model on Prediction Accuracy of Welding Residual Stress in an Austenitic Stainless Steel Multi-pass Butt-Welded Joint. Journal of Materials Engineering and Performance, 26(4), pp.1494-1505. doi:10.1007/s11665-017-2626-6

[14] Yaghi, A. H., Hyde, T. H., Becker, A. A., Sun, W., Hilson, G., Simandjuntak, S., ... & Smith, D. J. (2010). A comparison between measured and modeled residual stresses in a circumferentially butt-welded P91 steel pipe. *Journal of Pressure Vessel Technology*, *132*(1), 011206. doi:10.1115/1.4000347

[15] Attarha, M. and Sattari-Far, I. (2011) 'Study on welding temperature distribution in thin welded plates through experimental measurements and finite element simulation', *Journal of Materials Processing Technology,* 211(4), pp. 688-694. doi:10.1016/j.jmatprotec.2010.12.003

[16] Fu, G., Lourenço, M.I., Duan, M. and Estefen, S.F., 2016. Influence of the welding sequence on residual stress and distortion of fillet welded structures. Marine Structures, 46, pp.30-55. doi:10.1016/j.marstruc.2015.12.001

[17] Lee, C., Chang, K. and Park, J. (2013) 'Three-dimensional finite element analysis of residual stresses in dissimilar steel pipe welds', Nuclear Engineering and Design, 256, pp. 160-168. doi:10.1016/j.nucengdes.2012.12.016

[18] Deng, D., Murakawa, H. and Liang, W. (2008) 'Numerical and experimental investigations on welding residual stress in multi-pass butt-welded austenitic stainless steel pipe', Computational Materials Science, 42(2), pp. 234-244. doi:10.1016/j.commatsci.2007.07.009

[19] Malik, A.M., Qureshi, E.M., Dar, N.U. and Khan, I. (2008) 'Analysis of circumferentially arc welded thin-walled cylinders to investigate the residual stress fields', Thin-Walled Structures, 46(12), pp. 1391-1401. doi:10.1016/j.tws.2008.03.011

[20] Cho, J. and Lee, C.H., 2016. FE analysis of residual stress relaxation in a girth-welded duplex stainless steel pipe under cyclic loading. International Journal of Fatigue, 82, pp.462-473. doi:10.1016/j.ijfatigue.2015.09.001

Highlights

- Three cases have been discussed and compared thermally and mechanically. Case A, a reference case, is a typical lined pipe welding including weld overlay and girth welding. Case B is a lined pipe welding without weld overlay. Case C is a pipe welding with just girth welding.
- Keeping the net heat input and other welding parameters constant, the maximum temperature at the welding centerline (WCL) in Case A is slightly higher than its counterparts in other cases.
- Comparing the three cases, the axial residual stresses at the fusion zone (FZ) on the inner surface are affected by the maximum temperature where higher temperatures produce higher levels of axial residual stress.